JOURNAL OF GEOPHYSICAL RESEARCH, VOL. 97, NO. C5, PAGES 7257–7269, MAY 15, 1992

Prediction of the Gulf Stream Path From Upstream Parameters

MEGHAN CRONIN, EVERETT CARTER,[1] AND D. RANDOLPH WATTS

Graduate School of Oceanography, University of Rhode Island, Narragansett

A linear Wiener (least squares optimal) filter is used to predict the path of the Gulf Stream in the region between Cape Hatteras and 70°W using upstream ("Inlet") conditions as filter inputs. Although position, angle, curvature, geostrophic velocity, and curvature vorticity (κv) measured at 73°W were tested as multiple Inlet parameters, it was found that Inlet position alone was the best predictor. With Inlet position as the predictor, this filter is equivalent to propagating meanders downstream with a typical phase speed and growth rate. Forecasts of the downstream path position are produced, more accurate than persistence, 12 days in advance at 140 km from the Inlet, 24 days in advance at 240 km from the Inlet, and 28 days in advance at 340 km from the Inlet.

1. INTRODUCTION

The Gulf Stream is an intense and highly variable current whose path remains coherent well into the Atlantic Basin. As the current separates from the coast near Cape Hatteras, the path forms wavelike features that propagate and grow in space and time. In our study region, between Cape Hatteras and 70°W, the meanders have wavelengths on the order of 200–400 km that propagate downstream at speeds of 10–30 km day^{-1} depending on the wavelength [*Watts and Johns*, 1982; *Vazquez and Watts*, 1985; *Tracey and Watts*, 1986].

The amplitude relative to the wavelength is small in the region between Cape Hatteras and 70°W; however the path envelope width grows from 40 km at Cape Hatteras to 80 km at 70°W [*Watts*, 1983]. This broadening of the envelope is in part due to annual and interannual shifting of the mean path [*Cornillon*, 1986; *Gilman*, 1988] as well as due to a downstream growth of the meander amplitude [*Halliwell and Mooers*, 1983; *Tracey and Watts*, 1986]. East of 70°W, the meander amplitudes become large relative to the wavelength, often pinching off to form rings.

We will show in this paper how the path position in the region between Cape Hatteras and 70°W can be predicted from upstream ("Inlet," near Cape Hatteras) conditions using a simple statistical filter, a linear Wiener least squares, optimal filter. Ultimately, proper dynamical models should improve upon this simple statistical filter. In particular, this statistical model is unable to account for path variations that may arise due to upstream propagation of meanders or due to interactions with rings downstream of the Inlet.

The idea that the path depends on upstream conditions, originated with *Warren* [1963]. *Robinson and Niiler* [1967] and *Niiler and Robinson* [1967] argued through conservation of vorticity that position, angle, curvature, and bottom velocity measured at some point along the stream could control the downstream path displacement.

Vazquez and Watts [1985] (hereinafter referred to as VW) tested the statistical dependence of the path on upstream position, angle, and curvature using linear response analysis techniques. The linear response model is equivalent to the Wiener filter but in the frequency domain instead of the time domain. Having calculated the coherences and transfer functions between the upstream and downstream displacements, VW were able to determine the phase speeds and growth rates of the meanders as a function of frequency. *Tracey and Watts* [1986] used this technique to measure the dispersion relationship using path data from an array of inverted echo sounders (IESs) in the region between Cape Hatteras and 70°W. Their results show that meanders are dispersive: short, high-frequency meanders travel faster than long, low-frequency meanders.

Our study is meant to complement the VW study. VW found that the Inlet parameters, position, angle, and curvature, should be able to predict 55–65% of the total path displacement variance within 300 km from the Inlet. The logical next step, which we take, is to actually predict the path displacement by working in the time domain. Note also that we are using an entirely different data set than VW with much finer resolution albeit smaller alongstream range.

2. CONSTRUCTING THE WIENER FILTER

Our notation will use a circumflex to distinguish the observed downstream displacement y from the predicted filter output $\hat{y}$, and primes to denote perturbations from the mean.

The Wiener filter [*Wiener*, 1949; *Robinson*, 1967] assumes that the system (in our case, the downstream path position, y') responds linearly to the past and present variability of the input parameters. The response at time $t+\tau$, $y'(t+\tau)$, can therefore be modeled by appropriately weighting the past and present perturbations of the input parameters.

Suppose that the system depends upon the r input parameters, x_i, $i = 1, 2, \ldots, r$. If the input parameters are stacked in an input vector time series, $\mathbf{I(t)}$, such that each component of the vector is a demeaned input parameter at time t, e.g.,

$$\mathbf{I(t)} = \begin{bmatrix} x_1'(t) \\ x_2'(t) \\ \vdots \\ x_r'(t) \end{bmatrix} \tag{1}$$

then the predicted downstream displacement, $y'(\widehat{t+\tau})$, will be

Wiener filter

$$y'(\widehat{t+\tau}) = \sum_{n=0}^{p} \mathbf{w_n I(t\text{-}n)} \tag{2}$$

where $\mathbf{w}$ is a $(p+1)$ by r matrix whose row vectors $\mathbf{w_n}$ are the weights for each of the r parameters at time lag n. For a single

[1]Now at Naval Postgraduate School, Monterey, California.

Paper number 92JC00600.
0148-0227/92/92JC-00600$05.00

input parameter, r is 1 and $\mathbf{w_n}$ reduces to the scalar w_n. Equation (2) is the linear Wiener filter and represents a convolution between the input time series and the weights. Theoretically the convolution should extend to infinite time lags; however, for practical reasons, p is a finite number determined by the correlation time scale.

The mean square error (MSE) between the observed displacement and the Wiener filter output is

$$\text{MSE} = \left\langle \left(\widehat{y(t+\tau)} - y(t+\tau) \right)^2 \right\rangle \tag{3}$$

For an optimal filter, the mean square error is minimized with respect to the weights by setting the first derivatives to zero:

$$\frac{\partial}{\partial w_{ij}} \left\langle \left(\sum_{n=0}^{p} \mathbf{w_n I(t\text{-}n)} - y(t+\tau) \right)^2 \right\rangle = 0 \tag{4}$$

$$i = 0, 1, \cdots, p$$

$$j = 1, 2, \cdots, r$$

Solving this set of $r(p+1)$ equations (4) gives

$$< \mathbf{I}\,\mathbf{I}^T > \mathbf{w} - < \mathbf{I}\, y(t+\tau) >= 0 \tag{5}$$

from which the weights $\mathbf{w}$ can be found in terms of the autocorrelation matrix of the input paramters, $< \mathbf{I}\,\mathbf{I}^T >$, and the cross correlation vector between the downstream displacement and the input parameters, $< \mathbf{I}\, y(t+\tau) >$. Note that if the filter consists of $p+1$ weights for each of the r input variables, then the autocorrelation matrix will be a $r(p+1)$ by $r(p+1)$ matrix and the weight vector and the cross correlation vector will each have $r(p+1)$ components.

Provided that the input parameters are independent of each other, the autocorrelation matrix will be nonsingular and the system of equations described by equation (5) can be solved for the weights. To ensure that the estimation of the autocorrelation matrix is nonsingular, the sample rate of the convolution should be low enough that each weighted value of a given parameter is statistically independent, and the correlation at the maximum time lag should be statistically significant. For the Inlet path displacement, the optimal convolution sample rate is (4 days)$^{-1}$, approximately the highest frequency at which energetic meanders exist [*Tracey and Watts*, 1986]. Likewise, for the Inlet path displacement, the maximum time lag depends on the downstream distance and the propagation rate of the slowest energetic meander. Our filters all span approximately 1 month with the forecasting range increasing as the distance from the Inlet increases.

As long as the means and correlations remain independent of time (stationary), the filter weights determined from equation (5) will be optimal. Apparent nonstationarity could be, for example, due to long term variability or nonlinearities. In this paper, three cases are studied. In the first study, path data are assumed to be stationary: all perturbations are measured relative to their historic mean values, and the filter weights are constants.

In the second study, the stationarity assumption is relaxed to allow trends due to long term variability. The correlations are still assumed to be independent of time. Thus, in the second prediction scheme, constant weights are convolved with the detrended Inlet data to predict the downstream displacement from the trend. To predict the downstream position, the forecasted displacement must be added to an estimate of the downstream path trend.

In the third study, both the means and correlations are allowed to change slowly with time. The third prediction scheme is similar to the second; however, the filter is adaptive, and new weights are computed daily using the most recent covariances. Table 1 summarizes the fundamental differences between the three prediction schemes presented in this paper.

3. Filter Inputs: Inlet Parameter

Because water parcels are advected downstream and meanders propagate downstream in our study region, intuitively it makes sense that the downstream path depends upon upstream conditions, especially upon the upstream path displacement, as is demonstrated in the following thought experiment. Consider a nondispersive system where the meanders propagate downstream at a rate of x/τ and grow in amplitude at a rate of w/τ. Then the future displacement at a distance x from the Inlet can be forecasted using the present Inlet displacement, $y|_{x=0}$,

$$\widehat{y(t+\tau)}|_x = w y(t)|_{x=0} \tag{6}$$

If instead the meanders are dispersive, there will be a spread in energy about the time lag corresponding to the average propagation rate so that more weights are needed to predict the path:

$$\widehat{y(t+\tau)}|_x = \sum_{n=0}^{p} w_n y(t-n)|_{x=0} \tag{7}$$

Thus, when Inlet displacement $y|_{x=0}$ is used as an input, the Wiener filter is equivalent to propagating meanders downstream at optimal phase speeds and growth rates.

From the preceding discussion, it is clear that Inlet displacement should be a good predictor. Historical literature suggest that dynamically [*Robinson and Niiler*, 1967; *Luyten and Robinson*, 1974] and statistically [VW] the path depends on upstream angle and curvature as well as position. Curvature is suggested by these authors as a predictor because of its role in curvature vorticity. In addition, if either advection or baroclinic instability is important, then baroclinic geostophic velocity could be a good predictor. Therefore, in this study, Inlet position, angle, curvature,

TABLE 1. The Fundamental Differences Between the Three Prediction Schemes

Scheme	Assumption	Weights	Perturbation	Data Requirement
1	stationary	constant weights	Parameters are measured relative to historic mean	Once weights are determined, need real-time Inlet data to forecast downstream path
2	quasi-stationary	constant weights	Parameters are detrended	Once weights are determined, need real-time Inlet data and downstream path trend to forecast path
3	quasi-stationary	filter weights are time dependent (adaptive filter)	Parameters are detrended	Need real-time information on entire path to forecast the downstream path

geostophic velocity, and curvature vorticity have been tested as filter inputs.

4. THE DATA

The filter was tested on a continuous, 2-year (April 1983 to May 1985) inverted echo sounder data set from an array in the 460 km by 240 km box region between 74°W and 70°W shown in Figure 1. Although the data are historical, our study simulates real-time predictions. With telemetry IESs, the parameters could eventually be measured in real time, enabling this type of forecasting to be used as an operational prediction system.

IESs are bottom-moored instruments which monitor the depth of the main thermocline acoustically. For a detailed description of the instrument, the reader is refered to *Chaplin and Watts* [1984] and *Watts and Rossby* [1977]. Likewise, *Watts and Olson* [1978], *Watts and Johns* [1982], and *Tracey and Watts* [1986] have thoroughly described the techniques used to convert the acoustic travel time to the depth of an isotherm in the high-gradient part of the main thermocline. In our study, the IESs have monitored the depth of the 12°C isotherm (Z_{12}). Because the current is a narrow, coherent jet in this region and the 400 m Z_{12} contour is roughly in the center of the jet, we will use the terms "stream path," "path," and "400-m Z_{12} contour" interchangably.

Objective analysis (OA) [*Carter and Robinson*, 1987; *Watts et al.*, 1989] of the IES data provides daily contour maps of the Z_{12} (thermocline) topography. The maps are oriented 064°T, approximately parallel to the historic mean path, where in our coordinate system, x is the downstream distance and y is the displacement from the historic mean. As can be seen in Figure 1, for this study, the "Inlet" is the cross-stream line, $x = 0$, through 73.5°W. Thus, the "Inlet" displacement (relative to the historic mean), $y|_{x=0}$, is the $(x = 0, y)$ coordinate of the 400-m Z_{12} contour. The uncertainty of the IES measured displacement is ±5 km.

Inlet angle, θ, and curvature, κ, are computed from a cubic spline of the stream path and have respective uncertainties of ±5° and $\pm 0.003 \times 10^{-3}$ m^{-1}. Recent work by *Kim* [1991] has extended the interpretation of the IES Z_{12} maps beyond a path indicator for the Gulf Stream to that of a stream function for the flow. Therefore, as a simple parameterization, the baroclinic geostrophic velocity, v, is $(g^*/f)(Z_{12}/y)$ where $g^* = 0.001$ m s^{-2} is the reduced gravity, f is the Coriolis parameter, Z_{12} is the difference between the Z_{12} measured 20 km onshore of the path and 60 km offshore, and $y = 80$ km. The uncertainty of this estimate of the mean geostrophic velocity is approximately ±0.05 m s^{-1}. Curvature vorticity is κv and has an uncertainty of approximately $\pm 0.2 \times 10^{-5}$ s^{-1}.

The Wiener filter is used to predict the 740-day displacement time series at 140 km, 240 km and 340 km (roughly one meander wavelength) downstream of the Inlet. Figure 2 shows all the relevant data: the five Inlet parameter time series and the three downstream displacement time series as measured by the IESs.

In all prediction schemes, the filter which predicts the 740-day downstream displacement time series, is constructed from a 150-day subset of the data. On the one hand, we wanted the subset to be sufficiently long to estimate the correlations. In general a record length of about a year is needed to estimate correlations with time lags of 36 days. On the other hand, our total data set is only 2 years. In order to maximize the period of time which is predicted by an independent filter, we wanted the subset to be a fraction of the total length of the time series. Our choice of 150 days is thus a compromise. With a longer data set, more data would have been used to construct the filters.

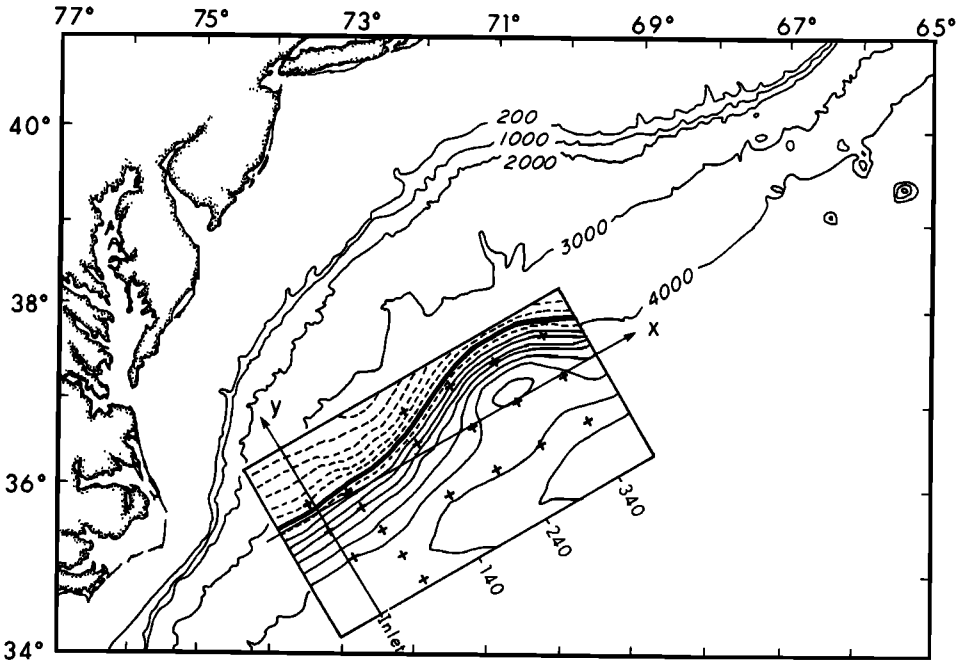

Fig. 1. An example of an objective analysis (OA) map of the thermocline topography superimposed upon a map of the western North Atlantic region. The depths of the 12°C isotherm are measured by an array of inverted echo sounders (IES). IES sites are indicated by plus marks. The first solid line is the 500-m contour of the 12°C isotherm and the contour interval is 50 m. The 400-m $Z12$ contour (which we refer to as the Gulf Stream path) is highlighted for clarity. The x axis of the OA map approximates the historical mean path. The y axis is what we refer to as the Inlet.

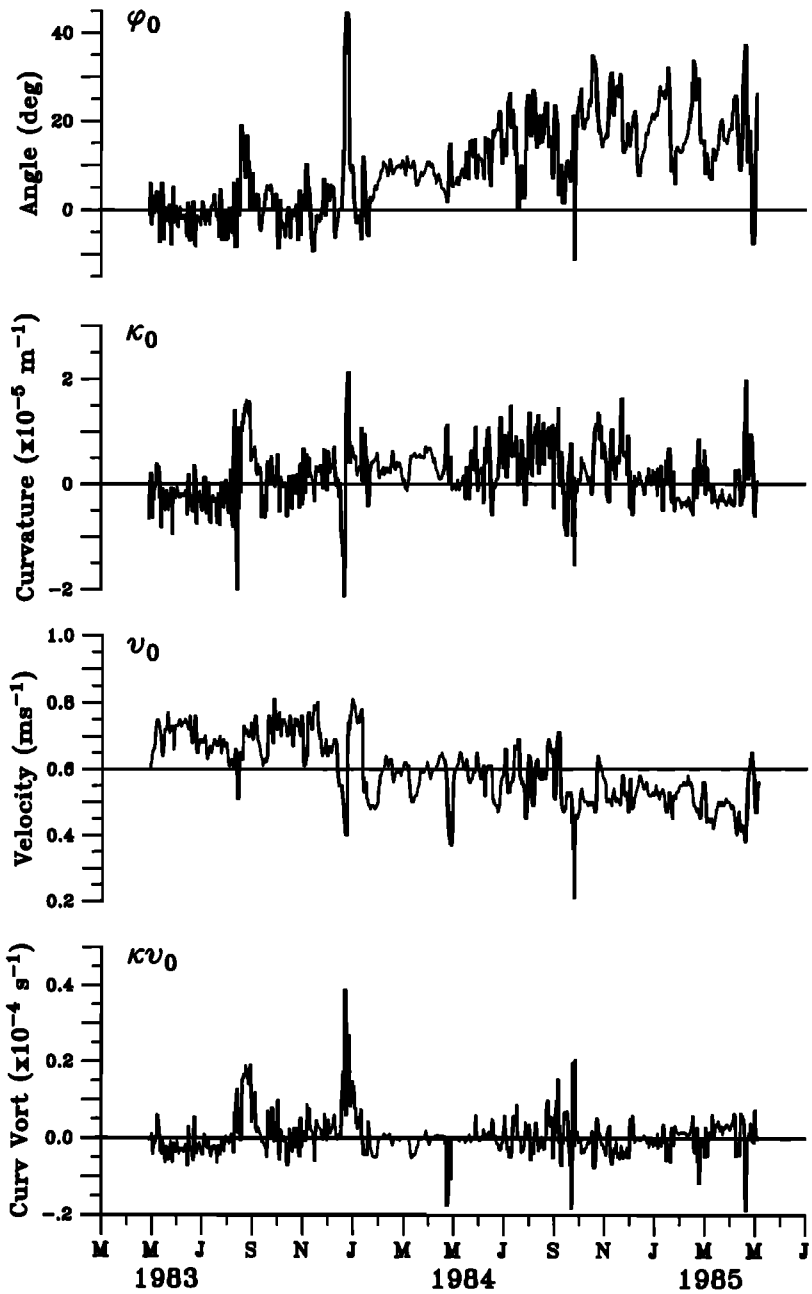

Fig. 2*a*. Inlet parameter time series (angle, curvature, velocity, and curvature vorticity), measured by the inverted echo sounder array.

5. The First Prediction Scheme: Perturbations Relative to Historic Mean; Constant Weights

In this first prediction scheme, the data are assumed to be stationary. That is, the means and correlations are assumed to be independent of time. Thus by equation (5), the weights will be independent of time and the parameters can be measured relative to their historical mean values. Examining the time series shown in Figure 2, the stationarity assumption might be violated by these time series. Nevertheless, this simple filter will be shown to be very successful.

The success of a predictor depends on how correlated the parameter is to the desired output. By shifting and overlaying the Inlet time series with the downstream displacements in Figure 2, it is clear that the Inlet position should be, and in fact is, the best predictor. Because the trends in the time series cause the correlations to be biased high, the correlations are not shown for this scheme.

Although one might expect that the predictions would become better by including more input parameters, we found that this usually makes the predictions noisier and less reliable. Likewise, further from the Inlet, increasing the number of lags past the dominant propagation time lag increases the error. Therefore the most successful filter uses only Inlet position as a predictor and spans 12 to 16 days. As described in section 3, this filter is equivalent to propagating meanders downstream at typical phase speeds, with the fastest waves radiating from the present Inlet position and the slowest radiating from the Inlet 12 to 16 days ago. Thus, the 12-day forecast at 140 km, the 24-day forecast at 240 km and the 28-day forecast at 340 km all include meanders propagating at rates of 6–12 km day^{-1}.

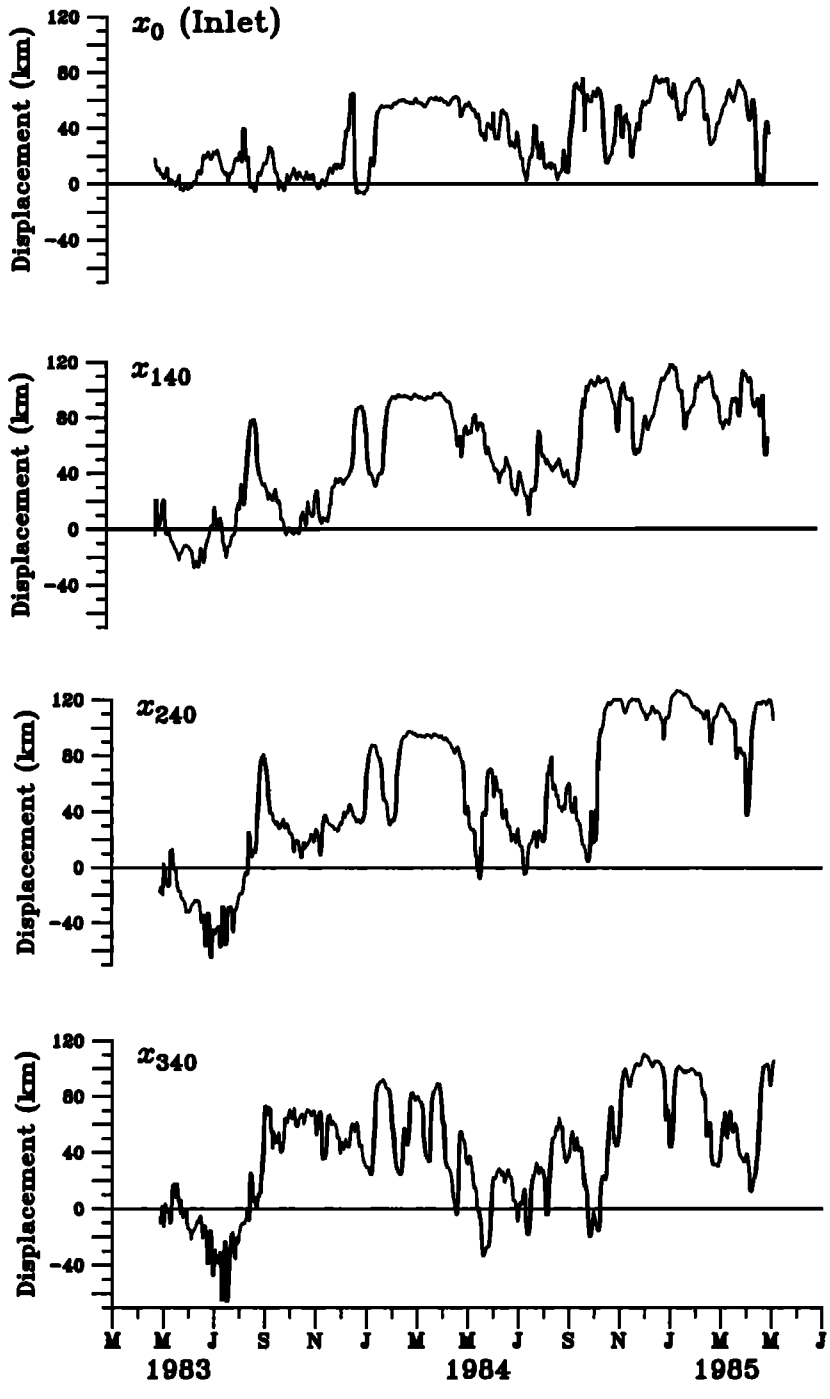

Fig. 2*b*. The displacement time series at the Inlet, and 140 km, 240 km, and 340 km from the Inlet, measured by the inverted echo sounder array.

As a result of the nonstationarity in the data, the success of the filter is highly dependent upon which 150-day segment of the record is used to construct the filter. The filters for all three distances were constructed according to equation (5) using the last 150 days of the 740-day time series.

5.1. *Prediction Scheme 1: 12-Day Forecast at 140 km*

The 12-day forecast of the displacement 140 km from the Inlet (about half a meander wavelength downstream) is shown in Figure 3. This very simple filter subsamples and weights the past 12 days of Inlet position at 4-day intervals:

$$\widehat{y(t+12)}|_{140} = 0.88y(t)|_0 + 0.09y(t-4)|_0 + 0.29y(t-8)|_0 + 0.33y(t-12)|_0$$

Because the amplitudes of the meanders increase with downstream distance, the sum of the weights is larger than 1.

As shown in Table 2, the standard deviation of the displacement signal, $\overline{q^2}$, is 39 km, while the rms error of the forecast, $\overline{\delta q^2}$, is only 20 km. Following *Davis* [1976], we define the skill index of the forecast as the fraction of the variance predicted:

$$Z = 1 - \frac{\overline{\delta q^2}}{\overline{q^2}}. \quad (8)$$

Thus, this filter has a skill index of 0.49. In other words, 49% of

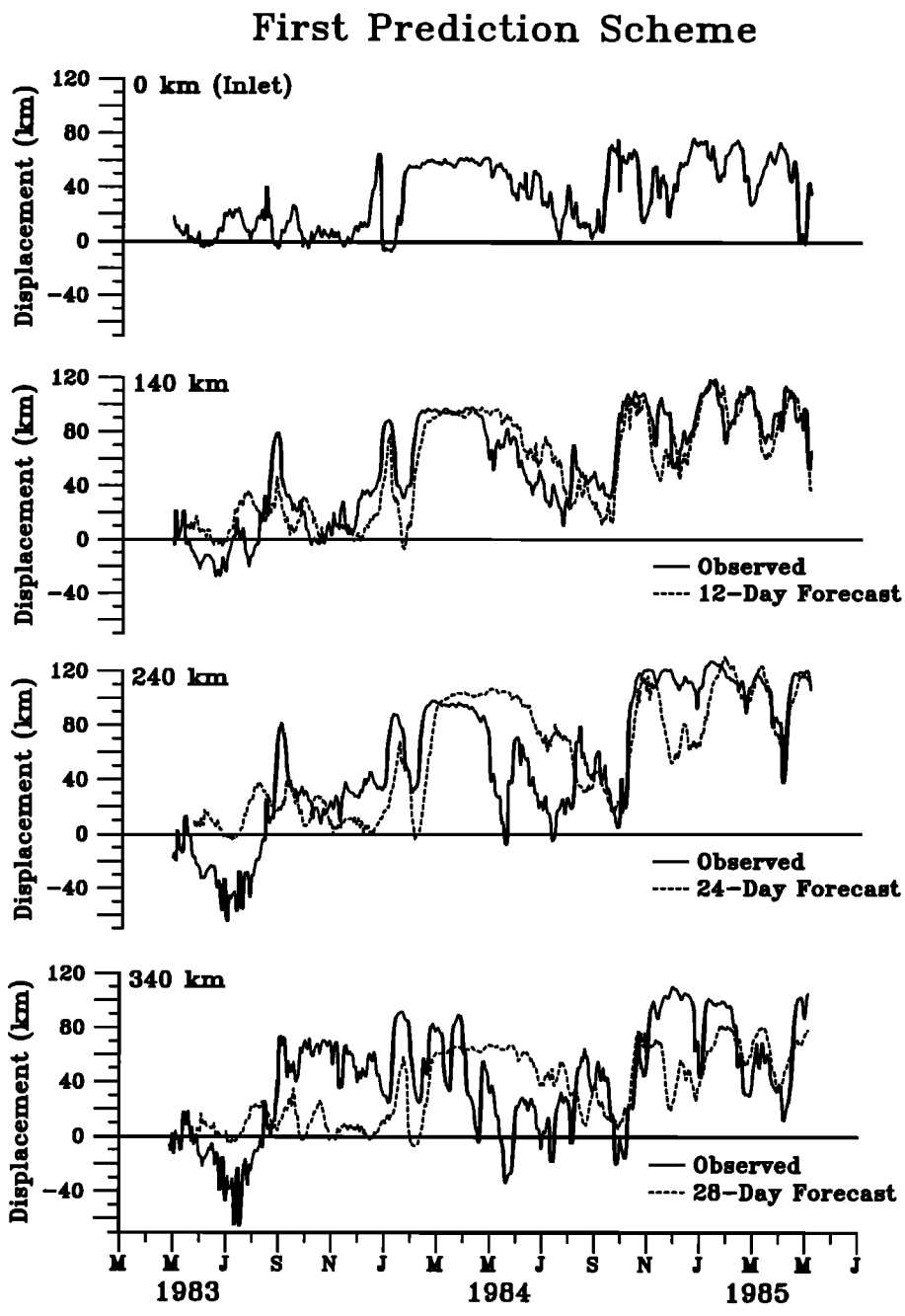

Fig. 3. The measured displacements (solid lines) and first scheme's forecasted displacements (dashed lines) at 140 km, 240 km, and 340 km from the Inlet. The measured Inlet displacement, which was used as a predictor, is shown in the top plot.

TABLE 2. Error Comparisons for Various Statistical Methods of Forecasting 12 Days Ahead the Path Position 140 km From the Inlet

12-Day Forecasts at 140 km	Root-Mean-Square Error, km	Skill Index
Prediction scheme 1	20.1	0.49
Prediction scheme 2	16.9	0.57
Prediction scheme 3	17.4	0.56
Persistence	20.5	0.48
Standard deviation	39.5	0

The skill index, defined in Equation (8), is the amount of variance predicted by the filter.

the variance at 140 km can be forecasted 12 days in advance. In our judgment, this is considerable success.

5.2. *Prediction Scheme 1: 24-Day Forecast at 240 km*

As can be seen in Figure 3, 100 km further downstream at 240 km from the Inlet, the 24 day forecast is still fairly good. The filter is given by

$$\widehat{y(t+24)}|_{240} = 0.49y(t)|_0 + 0.24y(t-4)|_0 + 0.28y(t-8)|_0 + 0.54y(t-12)|_0 + 0.20y(t-16)|_0$$

As Table 3 shows, the standard deviation of the signal is 50 km, while the rms error of this filter's forecast is only 35 km.

Thus 30% of the variance at 240 km can be forecasted 24 days in advance.

5.3. *Prediction Scheme 1: 28-Day Forecast at 340 km*

At 340 km downstream of the Inlet (70°W), the 28 day forecast is not good, as can be seen in Figure 3. The filter was constructed (as were the others) using the last 150 days of the 740-day time series. During this time period, the forecast is fairly good. But outside of this period, the signal generated by the filter is equivalent to noise (Table 4) .

To a large extent the discrepancy between the predicted and measured paths can be attributed to features which are present in the observations at 70°W but which do not originate at the Inlet. For example, in April 1984, there was a large meander trough downstream of our region at 68°W. This large meander trough pulled the entire path southward, causing considerable variability in the path position at 70°W. Because the filter uses only information from the Inlet, this type of variability at 70°W cannot be predicted by any of the schemes described in this paper.

TABLE 3. Error Comparisons for Various Statistical Methods of Forecasting 24 Days Ahead the Path Position 240 km From the Inlet

24-Day Forecasts at 240 km	Root-Mean-Square Error, km	Skill Index
Prediction Scheme 1	34.6	0.30
Prediction Scheme 2	30.6	0.38
Prediction Scheme 3	36.1	0.27
Persistence	35.0	0.29
Standard Deviation	49.5	0

TABLE 4. Error Comparison for Various Statistical Methods of Forecasting 28 Days Ahead the Path Position 340 km From the Inlet

28-Day Forecasts at 340 km	Root-Mean-Square Error, km	Skill Index
Prediction scheme 1	38.8	0.01
Prediction scheme 2	35.9	0.08
Prediction scheme 3	36.7	0.06
Persistence	36.6	0.06
Standard deviation	39.0	0

6. The Second Prediction Scheme: Trend Removed From Upstream and Downstream Parameters, Constant Weights

As was noted earlier, examining the trends of the data in Figure 2, it appears that the data are to some degree nonstationary. In this second prediction scheme the stationarity assumption is relaxed. It is assumed that the data contain low-frequency variability that appears as trends over the time scales of our prediction. The correlations of the detrended data, though, are assumed to be independent of time. Thus, by equation (5), the weights for this second scheme are still constants.

Because the prediction is intended to be done in real time, a causal high-pass filter is used to detrend the data. We used a second-order, 150-day high-pass Butterworth filter. Figure 4 shows the Inlet position decomposed into the low-frequency trend and the high-frequency variability:

$$y(t) = y_{LP}(t) + y'(t) \tag{9}$$

The correlations of the high-passed parameters are shown in Figure 5. Unlike scheme 1, these correlations fall to zero at long time lags, indicating that the detrending has successfully removed any biases. Inlet displacement is again the best predictor. Angle and curvature are correlated with downstream displacement only for time lags less than 10 days, making them poor predictors. Velocity is correlated with the downstream displacement at longer time lags; however, the correlation changes drastically from one period of time to another. Therefore, velocity is sometimes (but not always) a good predictor. Being a second-order derivative, curvature is a difficult parameter to measure and the presence of the noise in the curvature estimate could be partially responsible for the low correlations. Therefore, Inlet displacement is the only predictor used in the following forecasts.

The Wiener filter convolves the filter weights with the high-passed Inlet displacement to predict the the downstream displace-

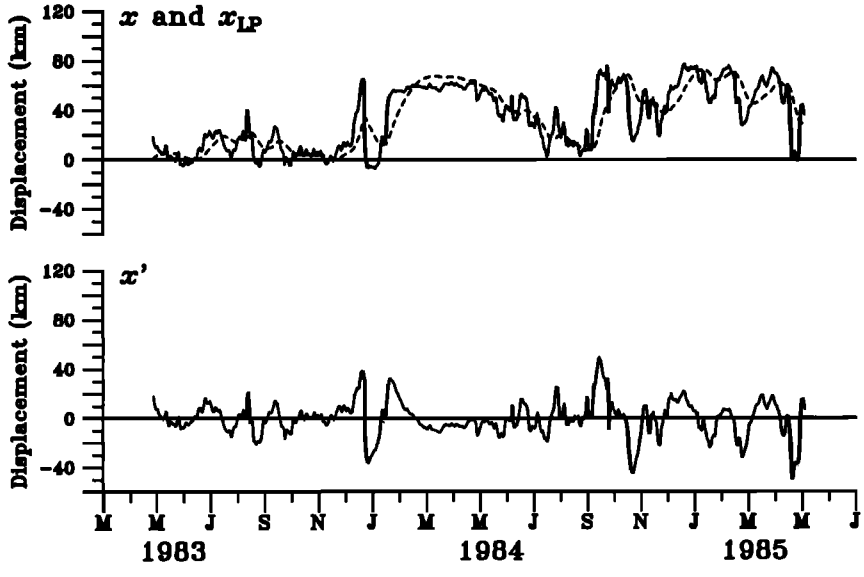

Fig. 4. The Inlet position time series (upper plot, solid line) decomposed into a trend (upper plot, dashed line) and a perturbation time series (lower plot) using a causal, second-order, 150-day high-pass Butterworth filter.

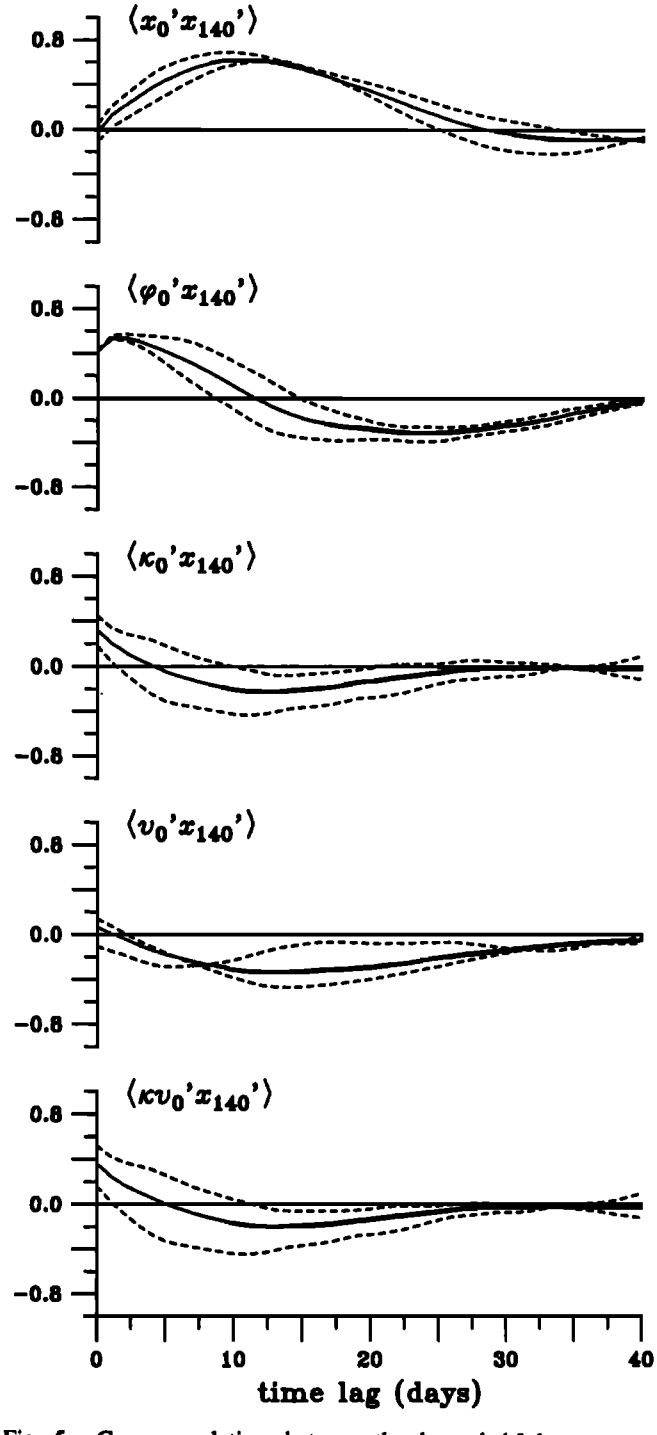

Fig. 5a. Cross correlations between the detrended Inlet parameters (Inlet displacement, angle, curvature, velocity, and curvature vorticity) and the time-lagged detrended displacement at 140 km from the Inlet. The solid lines are the cross correlations computed from the entire 740 days. The two dashed lines in each plot are the cross correlations computed from the first year and from the second year.

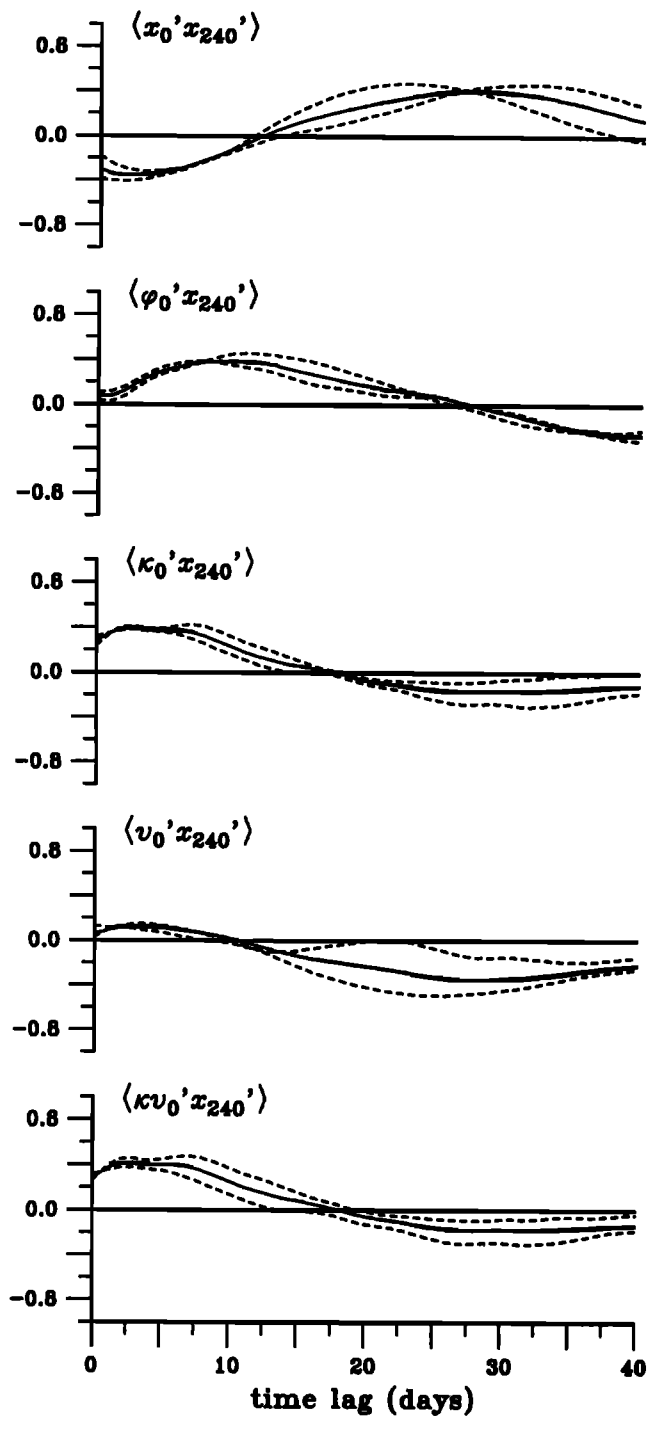

Fig. 5b. Same as Fig. 5a, except at 240 km from the Inlet.

ment $y'(\widehat{t+\tau})$. To forecast the downstream position $y(\widehat{t+\tau})$, an estimate of the future trend $y_{LP}(\widehat{t+\tau})$ must be added to the displacement forecasted by the Wiener filter. To estimate the future trend, real-time information on the downstream path must be available. Thus, this second prediction scheme is not as simple as the first, since it utilizes real-time information on the entire path.

Because in this case downstream path information is available, a simple way to predict the downstream path is through "persistence," i.e., assuming no temporal change in the path position:

Persistence

$$y(\widehat{t+\tau}) = y(t) \tag{10}$$

Note that persistence is equivalent to a phase shift in the time series. The redness of most geophysical spectra makes persistence an effective prediction method even in comparison with many dynamical models.

As discussed in Appendix 1, the difficulty in this second prediction scheme arises in estimating the future trend. We found

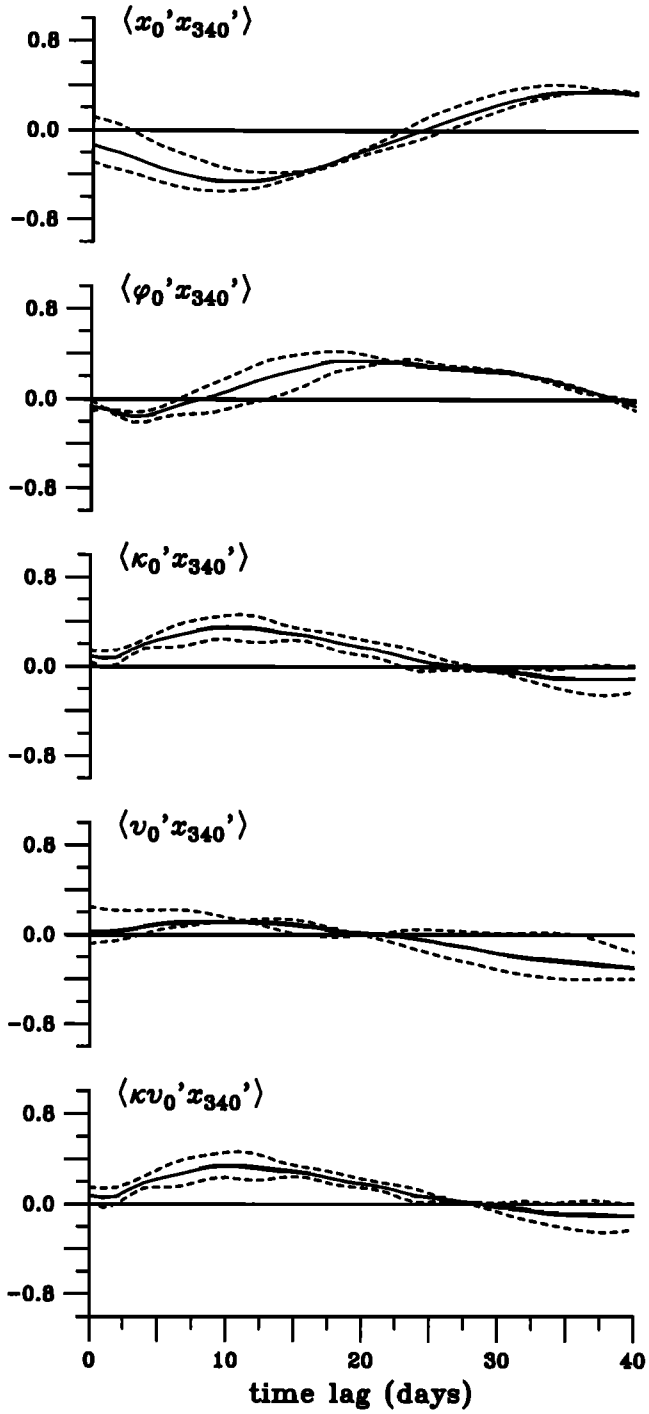

Fig. 5c. Same as Fig. 5a, except at 340 km from the Inlet.

that the best estimate of the future trend was persistence of the present position. Thus in the following sections, the future trend in the path position is approximated by the present path position:

$$\widehat{y_{LP}(t+\tau)} = y(t) \tag{11}$$

Because persistence is equivalent to a phase shift, this estimate of the future trend introduces an unavoidable phase shift between the forecasted time series and the observed time series, as will be seen in all forecasts of scheme 2.

At all distances for this second scheme, the filter weights are computed using the last 150 days of the high-passed data. The filter, represented by equation (2), subsamples and weights the high-passed Inlet displacement to forecast the downstream displacement. Finally, as is shown in equation (9), the estimate of the downstream trend (from equation (11)) must be added to the forecasted variability to obtain the forecasted downstream position.

6.1. *Prediction Scheme 2: 12-Day Forecast at 140 km*

This second scheme generates a 12-day forecast filter for 140 km downstream of the Inlet which is given by

$$\widehat{y(t+12)}|_{140} = y(t)|_{140} + 0.68y'(t)|_0 - 0.03y'(t-4)|_0 + 0.32y'(t-8)|_0 - 0.04y'(t-12)|_0$$

As is shown in Figure 6 , this forecast is quite good, with 57% of the variance at 140 km forecasted. The rms error of the 12-day forecast is 17 km, which is even better than the rms error of scheme 1's 12-day forecast (Table 2). Because in scheme 2 we have information on the present downstream path, we could have also used persistence as a prediction. Assuming persistence for 12 days, the rms error would be 21 km. Thus scheme 2's forecast at 140 km is better than persistence.

6.2. *Prediction Scheme 2: 24-Day Forecast at 240 km*

Scheme 2's filter which forecasts 24 days ahead the path position 240 km downstream of the Inlet is given by

$$\widehat{y(t+24)}|_{240} = y(t)|_{240} + 0.19y'(t)|_0 + 0.20y'(t-4)|_0 + 0.33y'(t-8)|_0 + 0.27y'(t-12)|_0$$

As is shown in Figure 6, this forecast is quite good, despite the phase shift introduced by the estimate of the future downstream trend, with 38% of the variance at 240 km forecasted 24 days in advance. The rms error of the forecast is 31 km, which again is better than the forecast of scheme 1 and is better than persistence. Assuming persistence for 24 days, the rms error would be 35 km.

6.3. *Prediction Scheme 2: 28-Day Forecast at 340 km*

The second scheme's 28-day forecast at 340 km is strikingly better than the first scheme's forecast, as can be seen in Figure 6. The filter in this case is given by

$$\widehat{y(t+28)}|_{340} = y(t)|_{340} + 0.40y'(t)|_0 - 0.05y'(t-4)|_0 + 0.66y'(t-8)|_0 - 0.32y'(t-12)|_0$$

The rms error of the 28-day forecast is 36 km, which is better than the standard deviation of 39 km. Thus the skill index is above zero (8% of the variance is predicted). It is also slightly better than persistence of the path position. Assuming persistence of the path at 340 km for 24 days, the rms error would be 37 km.

7. The Third Prediction Scheme: Trend Removed, Time-Dependent Weights

In the third and final prediction scheme, it is assumed that the means and correlations vary slowly with time. As in the second prediction scheme, the trends in the upstream parameters and downstream postion are removed by a causal 150-day, second-order Butterworth high-pass filter. The best estimate of the future trend in the downstream position is then added to the forecasted downstream displacement to obtain the forecasted position. The best estimate of the future trend is, as before, the present downstream position.

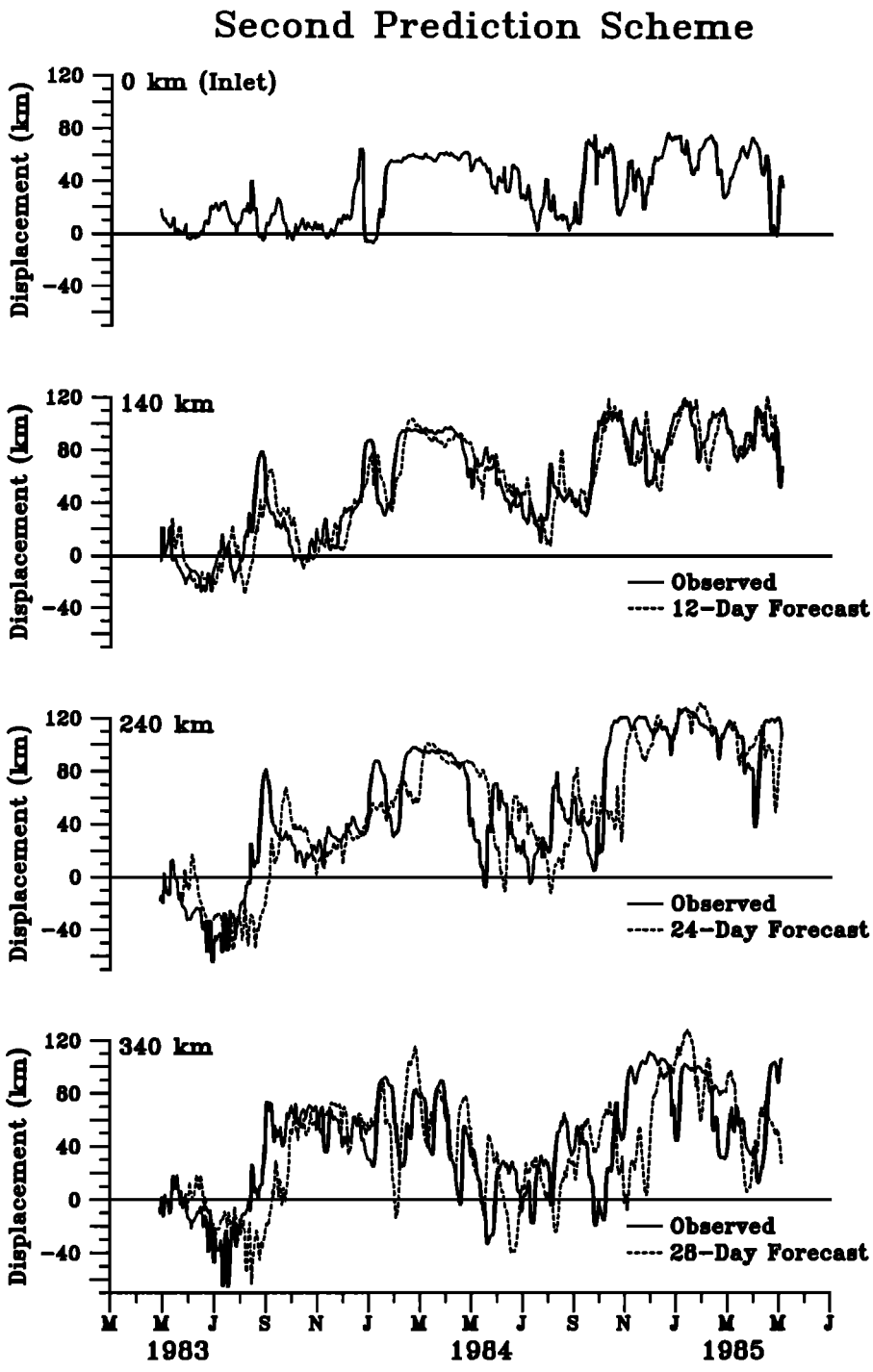

Fig. 6. The measured displacements (solid lines) and second scheme's forecasted displacements (dashed lines) at 140 km, 240 km, and 340 km from the Inlet. The measured Inlet displacement, which was used as a predictor, is shown in the top plot.

Unlike the first and second prediction schemes, in this third scheme, it is assumed that the correlations change slowly in time as can be noted from the dashed curves in Figure 5. Thus, because the autocorrelation matrix in equation (5) is time dependent, the optimal filter weights are determined from the most recent (detrended) data. This type of filter is called an adaptive Wiener filter and should not be confused with the Kalman filter; see Appendix 2.

Surprisingly, this more complicated prediction scheme is not as reliable as the second scheme in which the filter weights were constant. Therefore, scheme 3's forecasts are not shown, although the rms errors and skill indices are tabulated in Tables 2–4.

Because the filter is adaptive, the weights are time dependent, even changing sign as can be seen in the filter weights for the 12 day forecast at 140 km shown in Figure 7 . The constant weights of scheme 2 were computed from the last 150 days of the data and therefore are similar to the third scheme's weights at the last time step. The constant weights of scheme 2 are also very similar to the means of each time dependent weight of scheme 3, which is why scheme 2 is so successful.

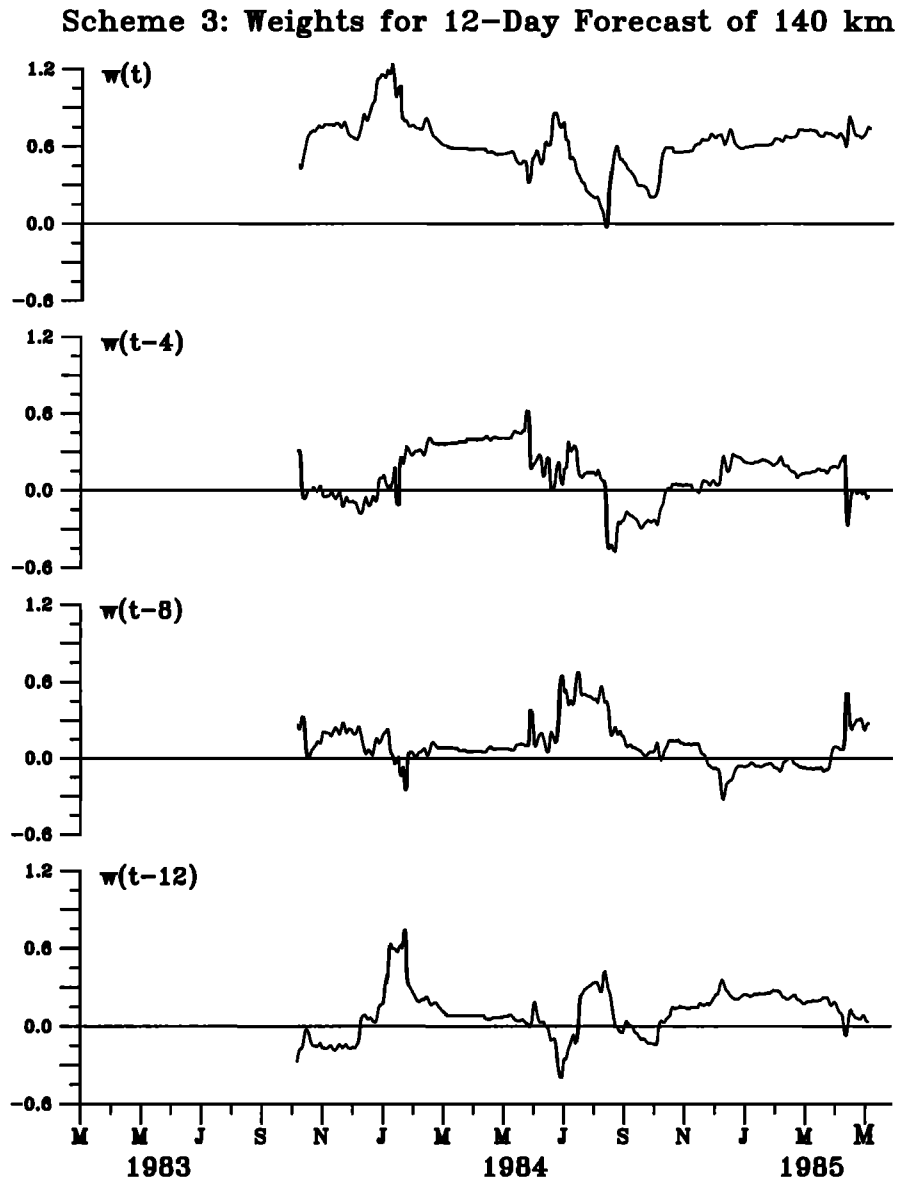

Fig. 7. Time series of filter weights for the third scheme's 12-day forecast at 140 km.

We believe that the adaptive filter (third prediction scheme) is not as reliable as the constant weight filter (second prediction scheme) because events which do not represent downstream propagating meanders, such as ring interactions, unavoidably get built into the filter. Whereas in the second prediction scheme, these events contaminate the forecast only during the period of the event (generally less than 1 month), in scheme 3, such events also contaminate the weights for the next 150 days.

8. Conclusions

Three prediction schemes were tested, each making different assumptions about the stationarity of the system. Scheme 1 assumes that the means and correlations are independent of time. Therefore, in the first scheme, the path displacements are measured relative to the historical mean path and the filter weights are constants. Once the filter weights are determined, the Wiener filter uses only information from the Inlet to forecast the downstream path. The effectiveness of this very simple filter is, in our judgment, remarkably good.

At any given time, the Gulf Stream path can be found with a respectively 68% (95%) confidence level in the plus and minus 1 (2) standard deviation envelope. Scheme 1, using only Inlet information, reduces this "prediction" envelope by nearly 40 km (80 km) at both 140 km and 240 km from the Inlet.

If downstream information is available, then the forecast can be improved further by using the second prediction scheme. Scheme 2 assumes that long term variability will cause the mean path to vary slowly, but that the correlations of the detrended data are independent of time. Thus, high-passed Inlet data are convolved with constant weights to forecast the downstream path displacement. An estimate of the future downstream trend is subsequently added to the forecasted displacement to forecast the downstream path position. This second scheme is not as simple as the first scheme because real-time information must be available for both the Inlet and the downstream position. Despite the phase shift introduced by the estimate of the future trend, the forecasts of scheme 2 are an improvement over the success of scheme 1 and are better than persistence.

The third scheme, using an adaptive Wiener filter in which the means and correlations change slowly in time, did not improve the reliability of the forecasts.

The best predictor was Inlet displacement. Angle, curvature, geostrophic velocity, and curvature vorticity measured at the Inlet were also tested as possible input parameters; however, the correlations were either poor, or highly variable (as in the case of velocity), or correlated with downstream displacements only for time lags less than 10 days (as in the case of angle and curvature). Therefore these parameters were poor predictors of the downstream path.

The prediction schemes presented here use Inlet (near Cape Hatteras) information to forecast the path position downstream to 71°–70°W. At 70°W, much of the variability is caused by ring-stream interactions and large amplitude meanders which originate downstream of the Inlet and therefore cannot be predicted from Inlet information.

In summary, this study shows that in the region between Cape Hatteras and 71°W, much of the variability in the path of the Gulf Stream can be forecasted using a Wiener filter with Inlet position as input. This very simple but effective filter is equivalent to propagating meanders at typical phase speeds and growth rates.

APPENDIX 1

Three different methods of estimating the future trend are tested against a noncausal 150-day low-pass filter estimate of the trend: (1) using an autoregressive filter on the past trend, (2) persisting the present trend into the future, and (3) persisting the present downstream position into the future. As is shown in Table 5, of these three estimates, the third (persistence of the present downstream position) is the best.

TABLE 5. Two Methods of Forecasting Trend Compared to True Low-Pass Trend

Test	Persisting Causal Trend Error, km	Persisting Position Error, km
12-Day Forecast Trend at 140 km	12.4	10.6
24-Day Forecast Trend at 240 km	26.8	21.6
28-Day Forecast Trend at 340 km	29.0	25.7

The true trend is computed using a 150-day symmetric (noncausal) low-pass filter (Butterworth run forward and backward); while the causal trend is estimated using a 150-day, second-order low-pass Butterworth filter.

The autoregressive (AR) filter is similar to the Wiener filter except that the input parameter is also the output parameter. Thus by equation (5), to predict a trend, the AR filter requires an extremely long time series to gain stable covariances. The AR predicted trend was for us, equivalent to noise.

The second method estimated the future trend by persisting the present trend. Because the forecast range (12–28 days) is a small fraction of the low-pass time scale (150 days), this would seem to be a good estimate. However, a phase shift is introduced into the trend by the causal high-pass filter. This phase shift proved to be serious when estimating the future trend by the present trend.

We found that the best estimate of the future trend was persistence of the present position, $y_{LP}\widehat{(t+\tau)} = y(t)$, as is discussed further in the text.

APPENDIX 2

The Kalman filter is simply the recursive form of the Wiener filter (equation (2)):

Wiener filter

$$y'\widehat{(t+\tau)} = \sum_{n=0}^{\infty} \mathbf{w_n I(t\text{-}n)} \tag{12}$$

Kalman filter

$$y'\widehat{(t+\tau)} = \sum_{n=0}^{p} \mathbf{f_n I(t\text{-}n)} + \sum_{n=1}^{p} g_n y'\widehat{(t-n)} \tag{13}$$

It is possible to convert the Kalman filter into a Wiener filter by taking the Z transform of the Kalman filter, dividing both sides by the transformed g weights, and then transforming back to time:

$$\mathcal{Z}[g]\mathcal{Z}[y] = \mathcal{Z}[f]\mathcal{Z}[I] \tag{14}$$

$$\mathcal{Z}[y] = \frac{\mathcal{Z}[f]}{\mathcal{Z}[g]}\mathcal{Z}[I] \tag{15}$$

$$y'\widehat{(t+\tau)} = \sum_{n=0}^{\infty} \mathcal{Z}^{-1}\left[\frac{\mathcal{Z}[f]}{\mathcal{Z}[g]}\right] I(t-n) = \sum_{n=0}^{\infty} \mathbf{w_n I(t\text{-}n)} \tag{16}$$

where the weights, w, are equal to $\mathcal{Z}^{-1}\left[\mathcal{Z}[f]/\mathcal{Z}[g]\right]$.

Acknowledgments. This work has been supported by the Office of Naval Research under contracts N00014-87K-0235 and N00014-90J-1568.

REFERENCES

Carter, E. F., and A. R. Robinson, Analysis models for the estimation of oceanic fields, *J. Atmos. Oceanic Technol., 4,* 49–74, 1987.

Chaplin, G., and D. R. Watts, Inverted echo sounder development, in *Oceans '84 Proceedings,* vol. 1, pp. 249–253, IEEE, New York, 1984.

Cornillon, P., The effect of the New England Seamounts on Gulf Stream meandering as observed from satellite IR imagery, *J. Phys. Oceanogr., 16,* 386–389, 1986.

Davis, R. E., Predictability of sea surface temperature and sea level pressure anomalies over the North Pacific Ocean, *J. Phys. Oceanogr., 6,* 249–266, 1976.

Gilman, C. S., A study of the Gulf Stream downstream of Cape Hatteras 1975–1986, M.S. thesis, 75 pp., Univ. of R.I., Kingston, 1988.

Halliwell, G. R., Jr., and C. N. K. Mooers, Meanders of the Gulf Stream downstream from Cape Hatteras 1975–1978, *J. Phys. Oceanogr., 13,* 1275–1292, 1983.

Kim, H.-S., An observational streamfunction in the Gulf Stream, M.S. thesis, 126 pp., Univ. of R.I., Kingston, 1991.

Luyten, J. R., and A. R. Robinson, Transient Gulf Stream meandering, II, Analysis via a quasi-geostrophic time-dependent model, *J. Phys. Oceanogr., 4,* 256–269, 1974.

Niiler, P. P., and A. R. Robinson, The theory of free inertial jets, II, A numerical experiment, *Tellus, 19,* 269–291, 1967.

Robinson, A. R., and P. P. Niiler, The theory of free inertial jets, I, Path and structure, *Tellus, 19,* 269–271, 1967.

Robinson, E. A., *Multi-Channel Time Series Analysis With Digital Computer Programs,* 298 pp., Holden-Day, San Francisco, 1967.

Tracey, K. L., and D. R. Watts, On Gulf Stream meander characteristics near Cape Hatteras, *J. Geophys. Res., 91,* 7587–7602, 1986.

Vazquez, J., and D. R. Watts, Observations on the propagation, growth, and predictability of Gulf Stream meanders, *J. Geophys. Res., 90,* 7143–7151, 1985.

Warren, B. A., Topographic influences on the path of the Gulf Stream, *Tellus, 15*, 167–183, 1963.

Watts, D. R., Gulf Stream variability, in *Eddies in Marine Science*, edited by A. Robinson, pp. 114–144, Springer-Verlag, New York, 1983.

Watts, D. R., and W. E. Johns, Gulf Stream meanders: Observations on propagation and growth, *J. Geophys. Res., 87*, 9467–9476, 1982.

Watts, D. R., and D. B. Olson, Gulf Stream ring coalescence with the Gulf Stream off Cape Hatteras, *Science, 202*, 971–972, 1978.

Watts, D. R., and H. T. Rossby, Measuring dynamic heights with inverted echo sounders: Results from MODE, *J. Phys. Oceanogr., 7*, 345–358, 1977.

Watts, D. R., K. L. Tracey, and A. Friedlander, Producing accurate maps of the Gulf Stream thermal front using objective analysis, *J. Geophys. Res., 94*, 8040–8052, 1989.

Wiener, N., *Time Series*, 163 pp., MIT Press, Cambridge, Mass., 1949.

E. Carter, Naval Postgraduate School, Monterey, CA 93940.

M. Cronin and D. R. Watts, Graduate School of Oceanography, University of Rhode Island, Narragansett, RI 02882.

(Received October 31, 1991;
accepted January 8, 1992.)